Journal of Materials Chemistry C

Highly Soluble Copper(I) Iodide Based Hybrid Luminescent Semiconductors Containing Molecular and One-dimensional Coordinated Anionic Inorganic Motifs

Journal:	*Journal of Materials Chemistry C*
Manuscript ID	TC-ART-12-2022-005479.R1
Article Type:	Paper
Date Submitted by the Author:	28-Jan-2023
Complete List of Authors:	Hei, Xiuze; Rutgers University, Chemistry and Chemical Biology Teat, Simon; LBNL, ALS Li, Meng; Brookhaven National Laboratory, Chemistry Department Bonite, Megan; Rutgers The State University of New Jersey Li, Jing; Rutgers The State University of New Jersey, Chemistry and Chemical Biology

ARTICLE

Highly Soluble Copper(I) Iodide Based Hybrid Luminescent Semiconductors Containing Molecular and One-dimensional Coordinated Anionic Inorganic Motifs

Received 00th January 20xx,
Accepted 00th January 20xx

DOI: 10.1039/x0xx00000x

Xiuze Hei,[a] Simon J. Teat,[b] Mingxing Li, [c] Megan Bonite [a] and Jing Li *[a]

Copper(I) iodide based inorganic-organic hybrid semiconductors are considered as promising materials for various optoelectronic applications. Here, by using imidazolium bridged benzotrizaoles as multidentate ligands, we designed and synthesized a series of All-In-One (AIO) type CuI hybrid materials that hold both ionic and coordinate bonds at the interface of organic and inorganic modules. Their structures range from 0D clusters to 2D extended networks built on various molecualr (0D) and chain-like (1D) anionic inorganic motifs that are interconnected through cationic ligands via multiple Cu-N bonds. Benifited from their unique bonding nature, all compounds exhibit high stability towards heat and moisture, and can be well dissolved in polar aprotic solvents. They emit low energy light spanning from yellow to red color (550-625 nm). The electronic structure, emission mechanim, and effect of different coordination modes on their photophysical properties were studied by both experimental and theoritical methods, which have provided insight into the structure-property relationship of these inorganic-organic semiconductors.

Introduction

Crystalline inorganic-organic hybrid semiconductor materials have continued to attract increasing attention due to their potential in optoelectronic applications, including but not limited to, photovoltaics,[1] light-emitting diodes (LED),[2-4] photodetectors,[5] and lasing.[6] These materials are made of inorganic and organic motifs and therefore possess a wide range of interesting properties inherited from both components. Moreover, synergetic features result from the interplay of two components are often observed, which are extrinsic to each counterpart alone.[7-9]

As an important and promising class of the inorganic-organic hybrid materials, copper(I) halide based hybrid semiconductors have shown substantial promise in photoluminescence (PL) related applications due to their facile synthesis, non-toxic nature, excellent optical properties and structural diversity.[10-12] Since the first investigation on the Cu_4I_4 cubane cluster based hybrid material in 1976,[13] great effort has been made to design and synthesize novel functional hybrid semiconductors based on copper halides.[14] Depending on the types of chemical bonds between the inorganic and organic components, copper halide hybrid structures can be divided into three subgroups. Subgroup 1 compounds are composed of neutral organic and inorganic motifs connected through pure coordinate bonds; Subgroup 2 compounds are made of inorganic anions and organic cations forming pure ionic bonds. Subgroup 3 compounds, or all-in-one (AIO) structures, are essentially the combination of Subgroup 1 and 2, with inorganic anions and organic cations further linked by coordinate bonds.[9, 15, 16] The AIO structures are particularly interesting because of their unique bonding characteristics. Using specially designed organic ligands containing both the cationic centre (quaternary N or P) and active binding sites for subsequent coordination to Cu, we have recently succeeded in obtaining a variety of different types of AIO structures.[17-21] The integration of the coordination bonds (from neutral structures) and ionic bonds (from ionic structures) in a single crystal lattice allows the AIO structures to inherit all the beneficial features from the two constituents, such as optical tunability, enhanced chemical and thermal stability, strong luminescence, and solution processability.[4, 9, 22-24] These desirable features render the AIO-type structures promising candidates for possible use in solution-processed thin-film devices, including eco-friendly lighting phosphors,[18, 19, 21] emitting layers of LED devices,[4] and luminescent solar concentrators (LSC).[24] On the other hand, in-depth study and understanding of the structural-property relationships in these materials is equally important and will be crucial in guiding the future efforts to further modify their structures and to enhance/optimize their properties. Based on these considerations, continued efforts in designing and investigating new AIO-type compounds with diversified structures and coordination modes are much needed to expand the database of their structures and properties.

[a] Department of Chemistry and Chemical Biology, Rutgers University, Piscataway, New Jersey 08854, USA. E-mail: jingli@rutgers.edu.
[b] Advanced Light Source, Lawrence Berkeley National Laboratory, Berkeley, CA 94720, USA.
[c] Center for Functional Nanomaterials, Brookhaven National Laboratory, Upton, NY, 11973, USA.

† Electronic Supplementary Information (ESI) available: ^{1}H NMR spectroscopic data, structural plots, PLE spectra and temperature-dependent PL decay curves, DFT calculation results. CCDC 2227207-2227211. See DOI: 10.1039/x0xx00000x

Herein, by exploiting imidazolium derivative bridged benzotriazoles as cationic ligands with multi-binding sites for the first time, we have synthesized five new AIO structures, ranging from 0D clusters to 2D layers. Six different anionic inorganic modules were identified, five of which have not been reported previously and coordinate with cationic organic ligands via two different coordination modes. The electronic structures, emission mechanisms, as well as the effect of different coordination modes on the photophysical properties of these compounds are investigated by both experimental and theoretical methods. With decomposition temperatures above 210 °C, all compounds are robust towards heat, and they are also highly resistant to moisture. All compounds emit low energy light in the yellow-red region (550-625 nm). Notably, all compounds are well soluble in polar aprotic solvents, making the facile solution-based thin-film fabrication possible.

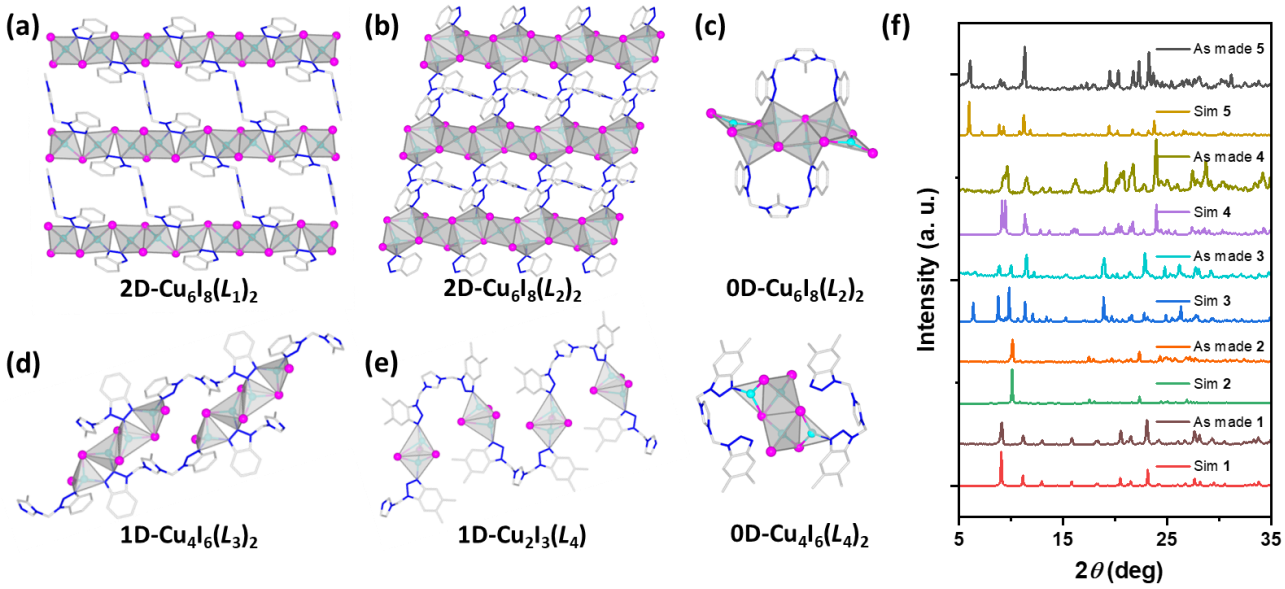

Fig. 1 Structural plots of the title compounds. (a) **1**, (b) **2**, (c) **3**, (d) **4**, and (e) **5**. Color scheme: gray: C; blue: N; cyan: Cu; purple: I. All H atoms and solvate molecules are omitted for clarity. (f) PXRD patterns of compounds **1-5**. From bottom to top: simulated **1**, as made **1**, simulated **2**, as made **2**, simulated **3**, as made **3**, simulated **4**, as made **4**, simulated **5**, and as made **5**.

Results and discussion

Design and synthesis of AIO compounds. To obtain AIO structures, the starting ligands must have available coordination sites to ensure the formation of dative bonds with Cu atoms, while maintaining their cationic nature to allow ionic interactions with the anionic inorganic modules. The cationic ligands used in previously reported AIO structures are mostly synthesized by alkylation of a tertiary amine or phosphine group, giving a terminal ammonium or phosphonium cationic centre with sp^3 hybridization.[4, 12, 17-20, 23, 25] Here, by substitution on the N atoms of imidazole-derivatives, four bidentate cationic ligands with sp^2 hybridized bridging imidazolium were prepared. The molecular structures of the ligands are shown in Figs. S1-4, along with ^{1}H NMR data to confirm their purity.

Solvothermal reactions of these ligands with Cu(I) iodide yielded high-quality single crystals of five new AIO-type hybrid compounds.[26, 27] The structures range from molecular (0D) clusters to layered (2D) networks with the following formulas: 2D-$Cu_6I_8(L_1)_2$ (**1**), 2D-$Cu_6I_8(L_2)_2$ (**2**), 0D-$Cu_6I_8(L_2)_2$ (**3**), 1D-$Cu_4I_6(L_3)_2$ (**4**), and $Cu_4I_6(L_4)_2$ (**5**).

Structural Description. The single-crystal X-ray analysis confirmed direct coordinate bonds between the free bonding sites (N atoms of benzotriazole, *bta*) of the cationic ligands and the Cu atoms of the anionic motifs. The crystallographic data are summarized in Table 1. All five structures are charge-neutral as shown in Fig. 1 and Fig. S5. While all four ligands share similar configurations, namely imidazolium linked two *bta*, six different anionic motifs ranging from 0D dimer ($Cu_2I_3^-$) to 1D chain ($Cu_6I_8^{2-}$) are obtained. Five of them have not been reported previously. Given similar ligands and different inorganic modules, this set of compounds serve as a good platform for our investigation of their structure and property relationships as detailed below.

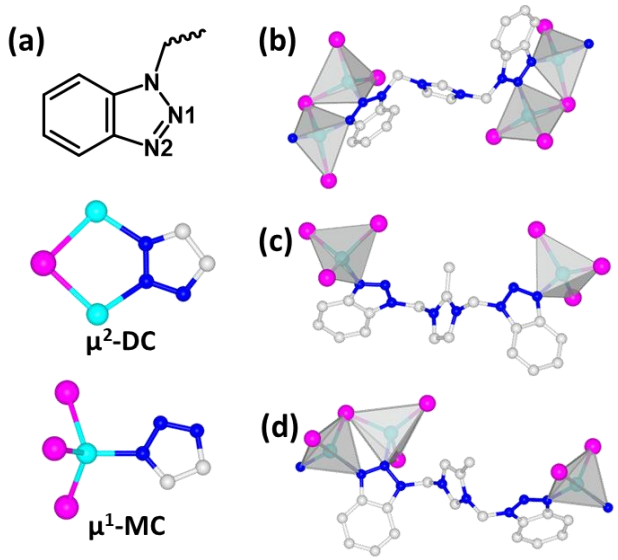

Fig. 2 (a) Top: structure of *bta* and bottom: illustration of μ^1-MC and μ^2-DC mode. Ligand coordination environments in (b) compound **1**, (c) compound **2** and (d) compound **4**. Color scheme: gray: C; blue: N; cyan: Cu; purple: I.

Table 1. Summary of crystal data of compounds **1-5**.

Compound	2D-$Cu_6I_8(L_1)_2$ (1)	2D-$Cu_6I_8(L_2)_2$ (2)	0D-$Cu_6I_8(L_2)_2$ (3) [a]	1D-$Cu_4I_6(L_3)_2$ (4) [a]	$Cu_4I_6(L_4)_2$ (5)
Empirical Formula	$C_{17}H_{15}Cu_3I_4N_8$	$C_{18}H_{17}Cu_3I_4N_8$	$C_{36}H_{34}Cu_6I_8N_{16}$	$C_{18}H_{17}Cu_2I_3N_8$	$C_{42}H_{46}Cu_4I_6N_{16}$
FW	1029.59	1043.61	2233.42	855.43	1790.51
Space Group	*Pnna*	*P* 21/c	*P* -1	*P* 21/n	*P* 21/c
***a* (Å)**	13.6626(8)	10.3623(3)	10.3781(4)	12.9449(13)	8.6527(9)
***b* (Å)**	13.9283(8)	17.4990(6)	10.8319(5)	13.5810(13)	16.0764(17)
***c* (Å)**	13.6877(8)	14.4300(5)	15.0528(6)	13.8160(13)	38.106(4)
α (°)	90	90	71.647(2)	90	90
β (°)	90	102.578(2)	72.550(2)	91.192(4)	90.414(4)
γ (°)	90	90	74.302(2)	90	90
V (Å³)	2604.7(3)	2553.79(15)	1502.90(11)	2428.4(4)	5300.6(10)
Z	4	4	1	4	4
***T* (K)**	100(2)	100(2)	100(2)	100(2)	100(2)
λ(Å)	0.7288	0.7288	0.7288	0.7288	0.7288
R_1	0.0184	0.0178	0.0224	0.0233	0.0276
wR_2	0.0453	0.0400	0.0567	0.0493	0.0661

[a] 2 molecules of Dimethylformamide (DMF) from **3**, 0.12 molecules of H_2O from compound **4** were removed from the formula.

Both compounds **1** and **2** are 2D extended networks composed of 1D-$Cu_6I_8^{2-}$ inorganic chains and 2-connected ligands. But their inorganic motifs have different structures. There are two coordination available N atoms in every *bta*, N1 and N2 (Fig. 2a). In compound **1**, both N1 and N2 atoms are involved in the formation of Cu-N dative bonds, giving a five-member ring with two adjacent Cu atoms and a bridging I atom (Fig. 2b). This is also noted as dicoordination mode (μ^2-DC).[18, 21] In contrast, only N1 atoms in compound **2** are coordinated to the inorganic motifs, giving a monocoordinated structure (μ^1-MC). Such a difference in the coordination mode may arise from steric hindrance. The added methyl group on the imidazolium tends to block the formation of N2-Cu dative bonds in compound **2** (Fig. 2c). In addition, reaction between L_2 and CuI under different conditions yields compound **3** as 0D clusters with a formula of 0D-$Cu_6I_8(L_2)_2$, adding another degree of structural diversity to this material family.

Compound **4** is a 1D chain type structure, made of discrete $Cu_4I_6^{2-}$ clusters and L_3. Interestingly, the two *bta* of L_3 adopt different coordination modes, differing from other compounds in which they adopt the same coordination mode to the inorganic motifs (Fig. 2d). This is possibly due to the reduced symmetry of L_3. While the *bta* further away from the methyl group takes the μ^2-DC mode, the one closer to the methyl group adopts the μ^1-MC mode. This behavior further confirms that the steric effect does play a role in the coordination modes of the resultant structures.

Compound **5** contains two independent components in the single crystal lattice, namely 1D-$Cu_2I_3(L_4)$ and 0D-$Cu_4I_6(L_4)_2$. Both are AIO type and have an overall neutral charge. Within the 1D chain, each Cu atom is tetrahedrally coordinated with three I atoms and one N atom from the ligand, and the two tetrahedra share one triangular face via three bridging I atoms. The overall coordination geometry of the Cu_2 dimer is trigonal bipyramidal. This inorganic motif has the same structure as that reported previously.[22] In the 0D cluster, the ligands are monodentate and coordinate to a single Cu atom.

Table 2. Summary of important physical properties

#	B. G. (eV)	PL_{max} (nm)	CIE	IQY [a] (%)	T_d [b] (°C)	Solubility [c] (mg/ml@RT)
1	2.4	610	(0.54, 0.44)	21	220	100
2	2.7	560	(0.44, 0.50)	15	240	190
3	2.9	550	(0.42, 0.54)	34	230	260
4	2.3	625	(0.56, 0.43)	38	220	140
5	2.4	590	(0.51, 0.46)	64	210	240

[a] λ_{ex} = 360 nm; [b] T_d: decomposition temperature; [c] Tested in DMSO at room temperature.

Most of the Cu atoms are tetrahedrally coordinated to I atoms and N atoms from the ligands in these structures, with a few exceptions. In compounds **3** and in 0D-$Cu_4I_6(L_4)_2$ of compound **5**, few Cu atoms are 3-coordinated to either I atoms and/or N atoms of the ligands. The coordination numbers of I atoms vary from 1 to 3. The Cu-N distances in these compounds range from 2.0 to 2.1 Å, similar to those of Subgroup 1 compounds containing only dative bonds.[28-30] The phase purity of all compounds was confirmed by powder X-Ray diffraction analysis (PXRD) as shown in Fig. 1f and Fig. S6.

Photophysical Properties. All five compounds emit low energy light centred between 550 nm and 625 nm under photoexcitation. The emission color ranges from yellow with Commission International del'Eclairage (CIE) chromaticity coordinates of (0.42, 0.54) to red with CIE coordinates of (0.56, 0.43). Their room temperature photoluminescence spectra are displayed in Fig. 3a-b and Fig. S7. The broad shape of the emission profiles indicates their radiative excited states are of charge transfer characteristics, similar to those observed in many other CuX-based hybrid materials.[31-33] The excitation-dependent emission spectra of all five compounds are plotted in Fig. 3c-d and Fig. S8. The emission intensities change as a function of excitation wavelength, while the shapes of their emission profiles remain the same, suggesting that the luminescence originates from a single excitation process. The internal quantum yields (IQYs) of these compounds

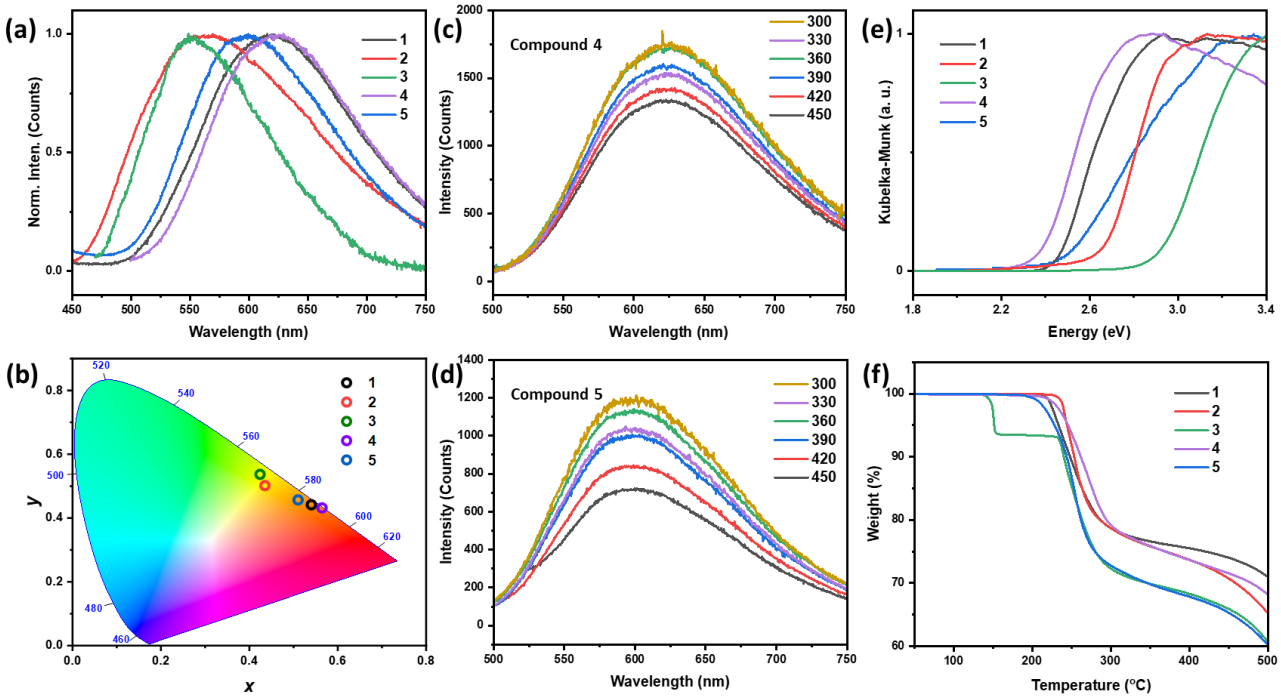

Fig. 3 (a) Normalized PL emission spectra (λ_{ex} = 360 nm) and corresponding (b) color chromaticity of all compounds. Excitation-dependent PL spectra of (c) compound **4** and (d) compound **5**. (e) Optical absorption spectra and (f) TG plots of all title compounds

were determined at room temperature under 360 nm excitation and are listed in Table. 2 and Figs. S9-10. The optical absorption spectra of compounds **1**-**5** were recorded at room temperature using diffuse reflectance spectroscopy. Their bandgaps were estimated from the absorption edges and range from 2.3 to 2.9 eV, as shown in Fig. 3e.

Thermogravimetric analysis (TGA) was conducted to evaluate the thermal stability of these compounds. All but compound **3** remained stable up to 210 °C (Fig. 3f). The weight loss of compound **3** at around 160 °C (~7%) is attributed to the loss of the solvated DMF molecules (Calc. 6.5 %). Above this temperature the weight losses are associated with loss of organic cations.[34, 35] As depicted in Fig. S11, after heating to 200 °C, the PXRD patterns and PL spectra of compounds **1** and **2** match well with those of the as-made samples, confirming their excellent structural stability.

Notably, all title compounds can be readily dissolved in polar aprotic solvents such as DMSO with similar solubility as those of other AIO compounds reported to date, despite that most of them are extended networks.[4, 18, 19, 21] Upon cooling or the introduction of antisolvents, these compounds can be recovered and regain their crystallinity. Compared to Subgroup 1 CuI-based extended structures which generally show very poor solubility in any common solvents,[28, 29, 36] such unique and desirable properties of AIO-type compounds demonstrate the distinct advantage in low-cost solution-processed high-quality thin film fabrications, enabling their applicability in LED, LSC and other energy-related devices.[9] Previous studies have suggested that this intriguing phenomenon is a result of introducing ionic bonds between the inorganic and organic motifs in coordinated networks.[9, 18, 19, 25]

To gain insight into the nature of photoluminescence in these compounds, the temperature-dependent lifetime decay curves of these compounds were collected from 78 K to 300 K. The lifetimes of these compounds show different temperature dependences based on their structures.

For both compounds **1** and **2**, which are 2D extended networks with infinite 1D inorganic chains, lifetimes increase significantly with decreasing temperature. (Fig. 4 and Fig. S12) Upon decreasing temperature, their lifetimes first increase slightly before 250 K and then increase sharply from 200 K to 100 K. Additionally, their photoluminescence decay curves are best fit by a biexponential decay function. (Tables S1-2) Using compound **1** as an example, the fraction of its fast decay constant τ_1 rises from 27.3% at 78 K to 82.7% at 300 K, while the fraction of the slow decay constant τ_2 decreases from 72.7% at 78 K to 17.3% at 300 K. All of the data are well compatible with the mechanism proposed by Yersin et al.,[37, 38] where both phosphorescence and thermally activated delayed fluorescence (TADF) are responsive for their emissions. Such phenomenon has been observed in many other previously reported CuX-based hybrid materials with small energy differences between the lowest excited singlet state (S_1) and the triplet state (T_1).[39, 40] As the temperature increases, a fraction of electrons can be thermally populated from T_1 back to S_1 via reverse intersystem crossing (RISC), and then follow a S_1 to S_0 radiative transition. (Fig. 4c) The relationship between the observed decay time (τ_{obs}) and absolute temperature (T) can be given as equation 1:

$$\tau_{obs} = \frac{3 + e^{-\frac{\Delta E(S_1-T_1)}{k_B T}}}{\frac{3}{\tau(T_1)} + \frac{1}{\tau(S_1)} \times e^{-\frac{\Delta E(S_1-T_1)}{k_B T}}}$$

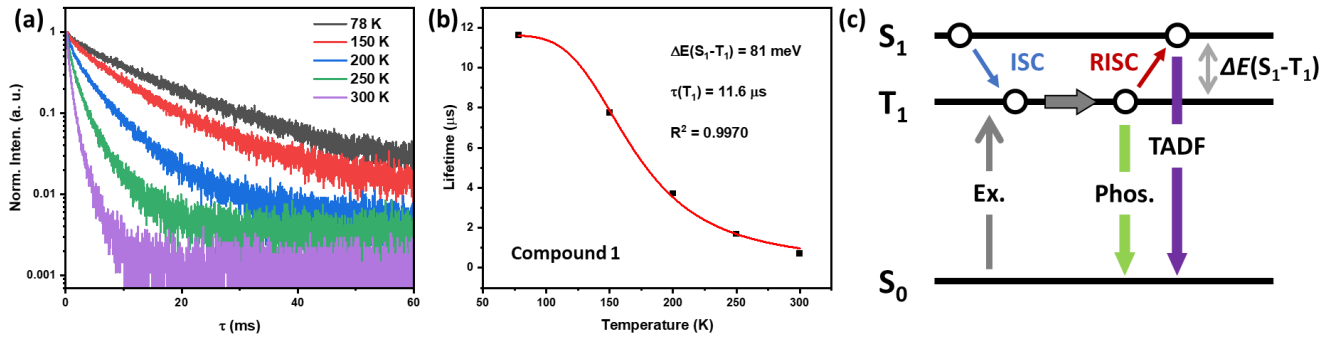

Fig. 4 (a) Temperature dependent luminescence decay curves of compound **1**. (b) The observed decay times of compound **1** and the fitting curve according to eq. 1. (c) Scheme depicting the radiative processes of phosphorescence (Phos.) and TADF.

ARTICLE

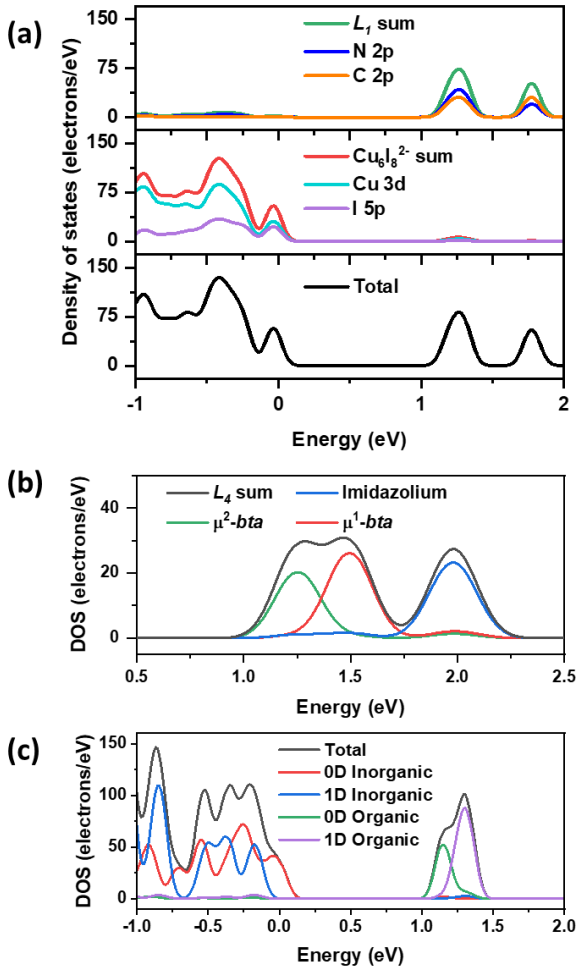

Fig. 5. (a) Calculated TDOS and PDOS of compound **1**. (b) Zoom in image of the conduction band region of compound **4**. (c) Distribution of different components in compound **5**.

Where $\tau(T_1)$ and $\tau(S_1)$ are the radiative decay times from the S_1 and T_1 states, respectively, k_B is Boltzmann's constant, T is temperature, and $\Delta E(S_1\text{-}T_1)$ is the energy difference between the two states. As shown in Fig. 4b and Fig. S12, excellent fittings of the decay times of compounds **1** and **2** were obtained, with coefficient of determination (R^2) values of 0.997 and 0.995, respectively. Derived from the equation, the $\Delta E(S_1\text{-}T_1)$ are determined to be 0.081 eV (653 cm^{-1}) for compound **1** and 0.070 eV (564 cm^{-1}) for compound **2**. Those numbers are comparable to that of other reported compounds with efficient TADF processes.[41-43]

Compound **4**, a 1D chain type structure made of desecrated inorganic clusters, behaves differently. Though its lifetime decay curves at various temperatures were well fitted with biexponential decay function, indicating two different processes contribute to its emission, the fraction of fast and slow decay components stay insensitive toward temperature changes (Fig. S13). A fast decay fraction of ~10% and a slow decay fraction of 90% were observed for all tested temperatures, suggesting the two processes are both phosphorescence (Table S3). The two different emission processes may arise from the interesting coordination environment of the ligands. As mentioned above, the two *bta* in each ligand adopt different coordination modes when coordinated to the inorganic modules in compound **4**, namely μ^1-MC and μ^2-DC. The differently overlapped frontier orbitals will certainly differentiate the charge transfer rate constants as suggested in previous studies,[38, 41, 44] and thus lead to two emission processes with different decay times.

Interestingly, though compound **5** contains two independent AIO components [1D-$Cu_2I_3(L_4)$ and 0D- $Cu_4I_6(L_4)_2$], its PL lifetimes at different temperatures are best fit by monoexponential functions (Fig. S14 and Table S4). The observed lifetime decreases from 14 μs at 78 K to 4 μs at 300 K and does not align with Boltzmann distribution. This data suggests that only one component is responsible for the emission. As the Cu_2I_3 dimers are reported to have a much longer photoluminescence lifetime (~200 μs) at 77 K,[22] the emission is attributed to the 0D-$Cu_4I_6(L_4)_2$ clusters.

Electronic band structures. To understand the emission mechanisms, density functional theory (DFT) calculations were conducted to calculate the projected density of states (PDOS) for all five compounds using the Cambridge Serial Total Energy Package (CASTEP).[45] As shown in Fig. 5a and Figs. S16-19, despite that all five compounds are made of various inorganic motifs and different dimensionalities, their PDOS clearly reveal common features. The atomic states that contribute to the valence band maximum (VBM) are mostly from the inorganic components (Cu 3*d* and I 5*p* orbitals). On the other hand, their conduction band minimum is primarily made up of the atomic orbitals from organic ligands (C 2*p* and N 2*p* orbitals). Therefore, the emission mechanism of all compounds can be described as a combination of metal-to-ligand charge transfer (MLCT) and halide-to-ligand charge transfer (XLCT), or (M+X)LCT. Such emission mechanisms grant these materials with facile optical tunability by altering the lowest unoccupied molecular orbital (LUMO) energies of the used ligands, so that the emission energies and bandgaps of afforded hybrid materials can be systematically regulated.[46, 47] The solvated DMF molecules in compound **3** do not contribute to the frontier orbitals as shown in Fig. S13, and thus do not contribute to the emission process.

Further analysis of the calculated CBM region suggests that the ligand contribution comes from the *bta* that is coordinated to inorganic motifs (Figs. S15-17). The middle imidazolium spacers demonstrate much higher energy levels than the CBM (e.g., 0.55 eV, 0.6 eV and 0.9 eV higher in compounds **1**, **2** and **3**, respectively), and thus are not involved in the charge transfer process and only serve as cationic centers to ensure the formation of ionic bonds. The energy difference between *bta* with different coordination modes was successfully captured by the calculations. As depicted in Fig. 5b, the energy level of the contribution from μ^1-*bta* is slightly higher than that of μ^2-*bta*. This further confirms that two different radiative decay channels can be generated in compound **4**, agreeing with the photoluminescence decay time data. In addition, it is evident that both the lower-energy portion of the conduction band and higher-energy portion of the valence band of compound **5** are primarily populated by the 0D-$Cu_4I_6(L_4)_2$ clusters as shown in Fig. 5c. This result suggests that compared to that of the 1D-$Cu_2I_3(L_4)$ component, both the excitation and emission processes of the 0D-$Cu_4I_6(L_4)_2$ clusters are more energy-favourable. Therefore, the emission of compound **5** tends to be dominated by its 0D-$Cu_4I_6(L_4)_2$ component, echoing with our assignment based on the PL lifetimes.

Conclusions

In summary, a series of AIO-type CuI based organic-inorganic hybrid materials containing both coordinate and ionic bonds has been synthesized. These structures range from 0D clusters to 2D networks with a wide variety of anionic inorganic modules, which further coordinate to cation ligands via two different modes. The steric effect of the ligands on their coordination mode has been successfully captured. All compounds show high resistance to heat with decomposition temperature over 210 °C and are well soluble in polar aprotic solvents, as a result of their unique bonding nature. All compounds emit low energy light (550-625 nm) under excitation. Their emission mechanisms, electronic structures, and effect of coordination modes on their photophysical properties were investigated both experimentally and theoretically, suggesting that different coordination modes can yield alternative decay channels as a result of differently overlapped orbitals. This work provides insights in understanding the structure-property relationships of the AIO-type CuI based inorganic-organic structure family.

Experimental Section

Materials. 1H-benzo[1,2,3]-triazole (99%, Alfa Aesar); 5,6-dimethyl-1H-benzo[d][1,2,3]triazole (99%, Sigma-Aldrich); Formaldehyde (37% in aqueous solution, Alfa Aesar); Thionyl chloride (99%, Alfa Aesar); Imidazole (98%, TCI); 2-Methylimidazole (98%, TCI); 4-Methylimidazole (98%, TCI); Sodium hydroxide (97%, BDH); Potassium iodide (99%, Alfa Aesar); Acetone (99.5%, VWR); Acetonitrile (99.5%, VWR); Ethyl ether (99%, Fisher); Copper iodide (98%, Alfa Aesar); sodium salicylate (99%, Merck).

Preparation of 1,3-bis((1H-benzo[d][1,2,3]triazol-1-yl)methyl)-1H-imidazol-3-ium iodide (L_1 I). 1-(Chloromethyl)-1H-benzo[d][1,2,3]-triazole (*Cl-mbt*) was prepared according to the reported procedures.[18] In a round bottom flask, *Cl-mbt* (1.67 g, 10 mmol), Imidazole (0.68 g, 10 mmol), NaOH (0.6 g, 15 mmol) and DMSO (15 ml) were charged and stirred for 1 day at 100 °C. The reaction mixture was then extracted with DCM, dried, and purified by chromatography to give pale yellow solid as 1-((1H-imidazol-1-yl)methyl)-1H-benzo[d][1,2,3]triazole (*imbt*). *Cl-mbt* (0.84 g, 5 mmol), acetone (20 ml) and KI (2 g) were added to another flask and stirred for 4 h before filtration. The filtrate was evaporated under reduced pressure and added with acetonitrile (100 ml) and *imbt* (1 g, 5 mmol). After refluxing overnight, the reaction mixture was evaporated under reduced pressure and washed with ethyl ether to yield pale yellow solid. Drying under vacuum and recrystallized with ethanol gives white solid as final product. The yield is 53%.

Preparation of 1,3-bis((1H-benzo[d][1,2,3]triazol-1-yl)methyl)-2-methyl-1H-imidazol-3-ium iodide (L_2 I). L_2 was prepared using similar procedure to L_1 but using 2-Methylimidazole. White solid was obtained with yield of 60%.

Preparation of 1,3-bis((1H-benzo[d][1,2,3]triazol-1-yl)methyl)-4ethyl-1H-imidazol-3-ium iodide (L_3 I). L_3 was prepared using similar procedure to L_1 but using 4-Methylimidazole. Pale yellow solid was obtained with yield of 57%.

Preparation of 1,3-bis((5,6-dimethyl-1H-benzo[d][1,2,3]triazol-1-yl)methyl)-1H-imidazol-3-ium iodide (L_4 I). L_4 was prepared using similar procedure to L_1 but using 5,6-dimethyl-1H-benzo[d][1,2,3]triazole. White solid was obtained with yield of 65%.

Synthesis of 2D-$Cu_6I_8(L_1)_2$ (1). CuI (28.5 mg, 0.15 mmol), L_1 I (23 mg, 0.05 mmol) and MeCN (4 ml) were sealed into a glass tube. The glass tube was kept in the 120 °C oven for 3 days and slowly cooled down to room temperature with rate of 5 °C/h. Block yellow single crystals along with pure phase crystalline powder were collected by filtration.

Synthesis of 2D-$Cu_6I_8(L_2)_2$ (2). Compound **2** was synthesized in the same way as that of **1**, using CuI and L_2 I. Block yellow single crystals with pure phase powdery samples were collected.

Synthesis of 0D-$Cu_6I_8(L_2)_2\cdot(DMF)_2$ (3). Compound **3** was synthesized using similar procedure to **2** but using mixture of MeCN (2 ml) and DMF (1 ml) as solvents. White block crystals were obtained by filtration.

Synthesis of 1D-$Cu_4I_6(L_3)_2$ (4). CuI (38 mg, 0.2 mmol), L_3 I (47 mg, 0.1 mmol), KI saturated aqueous solution (1 ml), water (1 ml) and MeOH (1 ml) were sealed in a glass tube, which was kept in 100 °C oven for 2 days before slowly cooling to room temperature (5 °C/h). Orange block crystals were obtained by filtration.

Synthesis of $Cu_4I_6(L_4)_2$ (5). Compound **5** was synthesized using similar procedure to **4** but using EtOH (3 ml) as solvent. Yellow needle single crystals were collected by filtration.

Synthesis of powder samples. Crystalline powder samples of all title compounds can be readily synthesized by reflux. Using the same solvent system and CuI/L feeding ratios as in the single

crystal growth, pure phase powdery samples can be obtained by filtration after refluxing overnight.

Single crystal X-ray diffraction (SCXRD). Single crystal data were collected using a D8 goniostat equipped with a Bruker PHOTON100 CMOS detector at the Advanced Light Source (ALS), Lawrence Berkeley National Laboratory, using synchrotron radiation. The structures were solved by direct methods and refined by full-matrix least-squares on F^2 using the Bruker SHELXTL package.[48]

Powder crystal X-ray diffraction (PXRD). Powder X-ray diffraction (PXRD) was carried out on a Rigaku Ultima-IV unit using Cu $K\alpha_1$ radiation (λ = 1.5406 Å), with a 2ϑ range of 3-35 ° and a scan rate of 2 °/min.

Thermogravimetric analysis (TGA). Q5000IR thermogravimetric analyser was used with nitrogen flow and sample purge rate of 10 and 25 ml/min, respectively. About 5 mg of samples were heated from room temperature to 500 °C at a rate of 10 °/min.

Photoluminescence measurements. Room temperature PL measurements were carried out on a Horiba Duetta fluorescence spectrophotometer. Temperature dependent time-resolved PL decays were recorded on a home-built time-correlated single photon counting instrument, with decays recorded in at least 1000 channels using a 410 nm long path filter.

Diffuse reflectance spectroscopy. Optical absorption of all compounds was recorded on a Shimadzu UV-3600 UV-Vis-NIR spectrometer at room temperature. The reflectance was converted to Kubelka-Munk function, $\alpha/S = (1-R)^2/2R$.

Internal quantum yield (IQY) measurements. IQYs were determined using a C9920-02 absolute quantum yield measurement system (Hamamatsu Photonics). Sodium salicylate was used as the standard with a reported IQY of 60%.

Solubility measurements. The solubility measurements were carried out at room temperature. About 50 mg of sample (fine powder) was loaded into a vail. DMSO was then added dropwise under sonication until the solution became clear and all solid dissolved. The amount of DMSO was recorded to calculate the solubility.

DFT calculations. The density of states of all compounds was calculated using the Cambridge Serial Total Energy Package with the crystal structures obtained from SCXRD. Generalized gradient approximations (GGA) with Perdew-Burke-Ernzerhof (PBE) exchange correlation functional (*xc*) were used for all calculations. The plane-wave kinetic energy cut-off was set as 351 eV and the total energy tolerance was set to be 1×10^{-5} eV/atom.

Conflicts of interest

There are no conflicts to declare.

Acknowledgements

The authors acknowledge the partial support from the U.S. Department of Energy, Office of Science, Office of Basic Energy Sciences (Grant No. DE-SC0019902). This research used the Advanced Light Source (ALS), which is a DOE Office of Science User Facility under contract No. DE-AC02-05CH11231. The temperature dependent luminescence work was carried out at the Center for Functional Nanomaterials, Brookhaven National Laboratory (BNL), which is supported by the U.S. Department of Energy, Office of Basic Energy Sciences, under Contract No. DE-SC0012704.

Notes and references

1. N. J. Jeon, J. H. Noh, W. S. Yang, Y. C. Kim, S. Ryu, J. Seo and S. I. Seok, *Nature*, 2015, **517**, 476-480.
2. M. D. Smith and H. I. Karunadasa, *Acc. Chem. Res.*, 2018, **51**, 619-627.
3. H. Cho, S.-H. Jeong, M.-H. Park, Y.-H. Kim, C. Wolf, C.-L. Lee, J. H. Heo, A. Sadhanala, N. Myoung, S. Yoo, S. H. Im, R. H. Friend and T.-W. Lee, *Science*, 2015, **350**, 1222-1225.
4. K. Zhu, Z. Cheng, S. Rangan, M. Cotlet, J. Du, L. Kasaei, S. J. Teat, W. Liu, Y. Chen, L. C. Feldman, D. M. O'Carroll and J. Li, *ACS Energy Lett.*, 2021, **6**, 2565-2574.
5. L. Dou, Y. Yang, J. You, Z. Hong, W.-H. Chang, G. Li and Y. Yang, *Nat. Commun.*, 2014, **5**, 5404.
6. Y. Jia, R. A. Kerner, A. J. Grede, B. P. Rand and N. C. Giebink, *Nat. Photonics*, 2017, **11**, 784-788.
7. V. W.-W. Yam, V. K.-M. Au and S. Y.-L. Leung, *Chem. Rev.*, 2015, **115**, 7589-7728.
8. B. Saparov and D. B. Mitzi, *Chem. Rev.*, 2016, **116**, 4558-4596.
9. X. Hei and J. Li, *Chem. Sci.*, 2021, **12**, 3805-3817.
10. K. Tsuge, Y. Chishina, H. Hashiguchi, Y. Sasaki, M. Kato, S. Ishizaka and N. Kitamura, *Coord. Chem. Rev.*, 2016, **306**, 636-651.
11. X. Zhang, W. Liu, G. Z. Wei, D. Banerjee, Z. Hu and J. Li, *J. Am. Chem. Soc.*, 2014, **136**, 14230-14236.
12. C. Chen, R.-H. Li, B.-S. Zhu, K.-H. Wang, J.-S. Yao, Y.-C. Yin, M.-M. Yao, H.-B. Yao and S.-H. Yu, *Angew. Chem. Int. Ed.*, 2018, **57**, 7106-7110.
13. C. L. Raston and A. H. White, *J. Chem. Soc., Dalton trans.*, 1976, DOI: 10.1039/DT9760002153, 2153-2156.
14. P. C. Ford and A. Vogler, *Acc. Chem. Res.*, 1993, **26**, 220-226.
15. W. Liu, Y. Fang and J. Li, *Adv. Funct. Mater.*, 2018, **28**, 1705593.
16. J.-S. Yao, J.-J. Wang, J.-N. Yang and H.-B. Yao, *Acc. Chem. Res.*, 2021, **54**, 441-451.
17. W. Liu, K. Zhu, S. J. Teat, G. Dey, Z. Shen, L. Wang, D. M. O'Carroll and J. Li, *J. Am. Chem. Soc.*, 2017, **139**, 9281-9290.
18. X. Hei, W. Liu, K. Zhu, S. J. Teat, S. Jensen, M. Li, D. M. O'Carroll, K. Wei, K. Tan, M. Cotlet, T. Thonhauser and J. Li, *J. Am. Chem. Soc.*, 2020, **142**, 4242-4253.
19. X. Hei, S. J. Teat, W. Liu and J. Li, *J. Mater. Chem. C*, 2020, **8**, 16790-16797.
20. A. V. Artem'ev, M. P. Davydova, X. Hei, M. I. Rakhmanova, D. G. Samsonenko, I. Y. Bagryanskaya, K. A. Brylev, V. P. Fedin, J.-S. Chen, M. Cotlet and J. Li, *Chem. Mater.*, 2020, **32**, 10708-10718.
21. X. Hei, K. Zhu, G. Carignan, S. J. Teat, M. Li, G. Zhang, M. Bonite and J. Li, *J. Solid State Chem.*, 2022, **314**, 123427.
22. H. Li, Y. Lv, Z. Zhou, H. Tong, W. Liu and G. Ouyang, *Angew. Chem. Int. Ed.*, 2022, **61**, e202115225.

23. L.-Z. Feng, J.-J. Wang, T. Ma, Y.-C. Yin, K.-H. Song, Z.-D. Li, M.-M. Zhou, S. Jin, T. Zhuang, F.-J. Fan, M.-Z. Zhu and H.-B. Yao, *Nat. Commun.*, 2022, **13**, 3339.
24. J.-J. Wang, C. Chen, W.-G. Chen, J.-S. Yao, J.-N. Yang, K.-H. Wang, Y.-C. Yin, M.-M. Yao, L.-Z. Feng, C. Ma, F.-J. Fan and H.-B. Yao, *J. Am. Chem. Soc.*, 2020, **142**, 3686-3690.
25. A. V. Artem'ev, E. A. Pritchina, M. I. Rakhmanova, N. P. Gritsan, I. Y. Bagryanskaya, S. F. Malysheva and N. A. Belogorlova, *Dalton Trans.*, 2019, **48**, 2328-2337.
26. W. Liu, Y. Fang, G. Z. Wei, S. J. Teat, K. Xiong, Z. Hu, W. P. Lustig and J. Li, *J. Am. Chem. Soc.*, 2015, **137**, 9400-9408.
27. Y. Fang, C. A. Sojdak, G. Dey, S. J. Teat, M. Li, M. Cotlet, K. Zhu, W. Liu, L. Wang, D. M. ÓCarroll and J. Li, *Chem. Sci.*, 2019, **10**, 5363-5372.
28. Y. Fang, K. Zhu, S. J. Teat, O. G. Reid, X. Hei, K. Zhu, X. Fang, M. Li, C. A. Sojdak, M. Cotlet and J. Li, *Chem. Mater.*, 2022, DOI: 10.1021/acs.chemmater.2c02490.
29. W. Ki, X. Hei, H. T. Yi, W. Liu, S. J. Teat, M. Li, Y. Fang, V. Podzorov, E. Garfunkel and J. Li, *Chem. Mater.*, 2021, **33**, 5317-5325.
30. Y. Fang, W. Liu, S. J. Teat, G. Dey, Z. Shen, L. An, D. Yu, L. Wang, D. M. O'Carroll and J. Li, *Adv. Funct. Mater.*, 2017, **27**, 1603444.
31. K.-H. Song, J.-J. Wang, L.-Z. Feng, F. He, Y.-C. Yin, J.-N. Yang, Y.-H. Song, Q. Zhang, X.-C. Ru, Y.-F. Lan, G. Zhang and H.-B. Yao, *Angew. Chem. Int. Ed.*, 2022, **61**, e202208960.
32. X. Hei, Y. Fang, S. J. Teat, C. Farrington, M. Bonite and J. Li, *Z. Naturforsch. B*, 2021, **76**, 759-764.
33. A. Tsuboyama, K. Kuge, M. Furugori, S. Okada, M. Hoshino and K. Ueno, *Inorg. Chem.*, 2007, **46**, 1992-2001.
34. J.-J. Shen, X.-X. Li, T.-L. Yu, F. Wang, P.-F. Hao and Y.-L. Fu, *Inorg. Chem.*, 2016, **55**, 8271-8273.
35. P. Hao, Y. Qiao, T. Yu, J. Shen, F. Liu and Y. Fu, *RSC Adv.*, 2016, **6**, 53566-53572.
36. W. Liu, D. Banerjee, F. Lin and J. Li, *J. Mater. Chem. C*, 2019, **7**, 1484-1490.
37. M. J. Leitl, V. A. Krylova, P. I. Djurovich, M. E. Thompson and H. Yersin, *J. Am. Chem. Soc.*, 2014, **136**, 16032-16038.
38. R. Czerwieniec, M. J. Leitl, H. H. H. Homeier and H. Yersin, *Coord. Chem. Rev.*, 2016, **325**, 2-28.
39. D. Volz, D. M. Zink, T. Bocksrocker, J. Friedrichs, M. Nieger, T. Baumann, U. Lemmer and S. Bräse, *Chem. Mater.*, 2013, **25**, 3414-3426.
40. R. Czerwieniec, J. Yu and H. Yersin, *Inorg. Chem.*, 2011, **50**, 8293-8301.
41. R. Hamze, J. L. Peltier, D. Sylvinson, M. Jung, J. Cardenas, R. Haiges, M. Soleilhavoup, R. Jazzar, P. I. Djurovich, G. Bertrand and M. E. Thompson, *Science*, 2019, **363**, 601-606.
42. G. Cheng, G. K.-M. So, W.-P. To, Y. Chen, C.-C. Kwok, C. Ma, X. Guan, X. Chang, W.-M. Kwok and C.-M. Che, *Chem. Sci.*, 2015, **6**, 4623-4635.
43. Y. Yang, N. Li, J. Miao, X. Cao, A. Ying, K. Pan, X. Lv, F. Ni, Z. Huang, S. Gong and C. Yang, *Angewandte Chemie International Edition*, 2022, **61**, e202202227.
44. J. Föller and C. M. Marian, *J. Phys. Chem. Lett.*, 2017, **8**, 5643-5647.
45. S. J. Clark, M. D. Segall, C. J. Pickard, P. J. Hasnip, M. J. Probert, K. Refson and M. C. Payne, *Z. Kristallogr. Cryst. Mater.*, 2005, **220**, 567-570.
46. P. C. Ford, E. Cariati and J. Bourassa, *Chem. Rev.*, 1999, **99**, 3625-3648.
47. L. Kang, J. Chen, T. Teng, X.-L. Chen, R. Yu and C.-Z. Lu, *Dalton Trans.*, 2015, **44**, 11649-11659.
48. G. Sheldrick, *Acta Crystallogr. C*, 2015, **71**, 3-8.